EFFECT OF HYDROGEN ON FATIGUE CRACK GROWTH RATE IN NATURAL GAS PIPELINES

Lappeenranta–Lahti University of Technology LUT

Master's Programme in Mechanical Engineering, Master's thesis

2024

Samuli Vilkki

Examiners: Associate Professor Hemantha Yeddu

Shahriar Afkhami, D.Sc. (Tech.)

ABSTRACT

Lappeenranta–Lahti University of Technology LUT

LUT School of Energy Systems

Mechanical Engineering

Samuli Vilkki

Effect of hydrogen on fatigue crack growth rate in natural gas pipelines

Master's thesis

2024

46 pages, 11 figures and 7 tables

Examiners: Associate Professor Hemantha Yeddu and D.Sc. (Tech.) Shahriar Afkhami

Keywords: hydrogen, hydrogen embrittlement, fatigue crack growth rate, natural gas pipeline

Hydrogen could be considered to be a clean energy option of the future, and it could possibly replace natural gas in many applications. The transportation of hydrogen gas through the existing natural gas transmission pipeline could bring significant cost savings if the existing infrastructure could be utilized. However, the effect of hydrogen on steel is considerably more harmful compared to natural gas. One well-known phenomenon related to this is hydrogen embrittlement.

The literature review of this thesis explains the basic theory on the relationship between steel and hydrogen and presents the different phenomena which can occur in steel in the presence of hydrogen. Differences between natural gas and hydrogen are also explained, especially from the perspective of using a natural gas pipeline.

Simulations and analysis part of this thesis presented an example of an existing natural gas pipeline, which was used for FEA to simulate the effect of fluctuating pressure load inside the pipeline with a presence of internal crack. The fatigue crack growth rate in pipeline steel with and without the presence of hydrogen was calculated. The results showed that hydrogen increases the crack growth rates in steels, in agreement with the literature.

TIIVISTELMÄ

Lappeenrannan–Lahden teknillinen yliopisto LUT

LUTin energiajärjestelmien tiedekunta

Konetekniikka

Samuli Vilkki

Vedyn vaikutus maakaasuputkien väsymissärön kasvunopeuteen

Konetekniikan diplomityö

2024

46 sivua, 11 kuvaa ja 7 taulukkoa

Tarkastajat: Apulaisprofessori Hemantha Yeddu ja TkT Shahriar Afkhami

Avainsanat: vety, vetyhauraus, väsymissärön kasvunopeus, maakaasuputkisto

Vetyä voidaan pitää tulevaisuuden mahdollisena puhtaana energiamuotona ja monissa käyttökohteissa sitä voitaisiin käyttää maakaasun korvikkeena. Vedyn siirtäminen käyttökohteisiinsa hyödyntämällä maakaasuputkistoa voisi tuoda merkittäviä kustannussäästöjä, jos jo olemassa olevaa infrastruktuuria voitaisiin hyödyntää. Vedyn vaikutukset teräkselle ovat kuitenkin huomattavasti haitallisemmat kuin maakaasun. Eräs tunnettu ilmiö tähän liittyen on vetyhauraus.

Työn kirjallisuuskatsaus selittää teräksen ja vedyn välisen vuorovaikutuksen taustalla olevan teorian perusteet, ja esittää erilaisia ilmiöitä, jota vedyn läsnäolo voi teräksessä aiheuttaa. Myös eroavaisuuksia maakaasun ja vedyn välillä avataan, erityisesti ottaen huomioon maakaasuputkiston hyödyntämisen.

Työn simulaatio- ja analyysiosuudet esittävät esimerkkimallin olemassa olevasta maakaasuputkesta, jota käytetään FE-analyysiin simuloimaan putken sisällä vallitsevan vaihtelevan paineen vaikutusta sisäisen särön läsnäolossa. Väsymissärön kasvunopeus putkiteräksessä vedyn läsnä ollessa ja ilman sen vaikutusta laskettiin. Tuloksista nähtiin vedyn särönkasvua lisäävä vaikutus, joka on linjassa myös kirjallisuuden kanssa.

SYMBOLS AND ABBREVIATIONS

Roman characters

C	Paris' Law material constant [MPa×mm$^{1/2}$]
C_H	Concentration of dissolved hydrogen [mol/m3]
da/dN	Rate of crack growth in relation to cycles [m/cycle]
P_{H_2}	Partial pressure of hydrogen [Pa]

Greek characters

ΔK	Stress intensity factor range [MPa×mm$^{1/2}$]

Dimensionless quantities

m	Paris' law material constant
R	Loading ratio
S	Solubility constant

Abbreviations

API	American Petroleum Institute
ASTM	American Society for Testing and Materials
BCC	Body-Centered Cubic
DVGW	Deutscher Verein des Gas- und Wasserfaches
FCC	Face-Centered Cubic
FEA	Finite Element Analysis
HEDE	Hydrogen-Enhanced Decohesion

HELP	Hydrogen-Enhanced Localized Plasticity Mechanism
HESIV	Hydrogen-Enhanced Strain Induced Vacancies
HIC	Hydrogen-Induced Cracking
HIPT	Hydrogen-Induced Phase Transformation
SCC	Stress Corrosion Cracking
SIF	Stress Intensity Factor

Table of contents

Abstract

Tiivistelmä

Symbols and abbreviations

1 Introduction 8
1.1 Background and context 8
1.2 Research problem and objectives 9
1.3 Justification of the study 9
1.4 Scope and limitations 9
2 Literature review 11
2.1 Solubility of hydrogen in steel 11
2.2 Lattice location of hydrogen 13
2.3 Crystallographic defects 13
2.3.1 Vacancies 13
2.3.2 Dislocations 13
2.3.3 Grain boundaries 14
2.4 Hydrogen theories 14
2.4.1 Hydrogen pressure theory 14
2.4.2 Hydrogen-induced phase transformation 15
2.4.3 Hydrogen-enhanced localized plasticity mechanism 15
2.4.4 Hydrogen-enhanced decohesion 15
2.4.5 Hydrogen-enhanced strain induced vacancies 16
2.5 Hydrogen embrittlement 16
2.6 Hydrogen-induced cracking 17
2.7 Stress corrosion cracking 19
2.8 Hydrogen attack 21
2.9 Hydrogen compared to natural gas 22
3 Methodology 24
3.1 Analysis specifications 24

3.2 FE-model setup 26
3.2.1 3D-model 26
3.2.2 Material parameters 27
3.2.3 Loads 28
3.2.4 Constraints 29
3.2.5 Crack properties 30
3.2.6 Mesh 31
3.2.7 Analysis settings 32
3.3 Fatigue crack growth rate plot 32
3.3.1 Natural gas 33
3.3.2 Hydrogen 33
4 Results 35
4.1 FEA results 35
4.2 Fatigue crack growth rate with natural gas as a medium 36
4.3 Fatigue crack growth rate with hydrogen as medium 36
5 Discussion 39
6 Conclusions 42
References 43

1 Introduction

The use of natural gas is in decline and hydrogen is considered as a potential replacement. This would greatly reduce the emissions, making it a more future-proof energy source. While natural gas already has an existing infrastructure to transport it to customer locations, hydrogen does not. As a result, a new transmission network would have to be constructed. Another option is to make use of existing natural gas pipelines, which could possibly reduce the costs (Télessy & Barner & Holz 2024, p. 821). The question is whether they are suitable for transporting hydrogen since there are many potential risks related. This thesis will focus on the risk of increased fatigue crack growth rate caused by hydrogen.

1.1 Background and context

There is already an existing natural gas transmission pipeline network in Finland, used for distributing gas for industry needs, energy production facilities, and fueling stations, for example. As can be seen already, the use of natural gas has been on a decline, and the same trend will continue in the future. As the use of one energy source is reduced, alternatives must be found and hydrogen is a potential option for this scenario, being significantly more environmentally safe.

However, hydrogen does not have a similar transmission network as natural gas in Finland, so one would have to be implemented from the ground up. Another interesting option would be to take advantage of the existing natural gas transmission pipeline network to use it for hydrogen transportation. Using this option, natural gas could be completely replaced by hydrogen in the network, or alternatively, the two could be mixed together. Using an existing infrastructure could reduce the costs of switching from the use of natural gas to hydrogen significantly, supposing there are no limiting factors, and the aim of this thesis is to answer some questions related to this.

1.2 Research problem and objectives

The research problem of the thesis arises from the fact that when changing the medium in a pipeline from natural gas to hydrogen, the effect of the new gas on the steel has to be examined in order to verify its suitability as hydrogen is known to be particularly prone to cause severe negative effects on steel and its mechanical performance (Nagumo 2016, p. 6).

The objective of the thesis is to understand what type of effect hydrogen has on steels and some theories behind it and to present comparable data which can be used to compare the consequences of a defect in a pipeline between the presence of natural gas and hydrogen in a similar scenario.

1.3 Justification of the study

The motivation for this master's thesis emerged from customer's interest in converting existing natural gas pipelines for hydrogen use. The possible reasons behind the rising curiosity might be for example the price increase of natural gas and the more environmentally friendly nature of hydrogen and thus possibly having more future potential when compared to natural gas.

1.4 Scope and limitations

The thesis can be divided into two parts: literature review and simulations and analysis part. The literature review consists of the necessary theory in order to understand the basic concepts behind the piping material conversion process, the main subject matter being hydrogen and its effect on pipeline steels and different phases of steel. Different failure mechanisms caused by the presence of hydrogen are also discussed. This section also includes the principle of hydrogen embrittlement and hydrogen-induced cracking. The intention is to keep the focus purely on topics directly related to hydrogen. There are also significantly more other subjects related to the conversion process as a whole, but due to the nature and extent of this work, they will not be the focus of this work and its literature review.

In the simulations and analysis part of the thesis, a common pipeline steel grade will be used as an example. Its specifications will be presented, and it will be used for FEA to simulate the effect of a fluctuating load inside the pipeline with the presence of an internal crack. The results will then be utilized to demonstrate the effect of hydrogen-induced cracking by forming fatigue crack growth rate plots for both natural gas and hydrogen, which can then be compared.

Even though this thesis is not intended to act as a definitive guide for carrying out such a project, it will still give a basic understanding of the topic, highlighting the effect of hydrogen on steels and answer questions related to the subject.

2 Literature review

This part of the thesis will focus on and examine the necessary theory behind the hydrogen piping conversion in order to be able to answer the research questions. Starting from the hydrogen itself and its effect on different phases of steel, proceeding to explain the different failure mechanisms present in the piping material.

2.1 Solubility of hydrogen in steel

When in contact with steel, hydrogen first physically absorbs into the surface layer as a H_2 molecule or H_3O^+ ion. This first phase of diffusion occurs quickly and is reversible, and the interaction's energy is as low as 3-5 kJ mol^{-1}. In the next step after the physical absorption comes the chemical absorption, where the atomic interactions take place in one atomic layer. Contrary to physical absorption, chemical absorption is not reversible and it is a more time-consuming process. Also, the interaction's energy is significantly higher at 40-160 kJ mol^{-1}. Final phase is the dissolution, where hydrogen atoms diffuse into the volume due to the gas' concentration gradient. (Nagumo 2016, p. 1; Li & Ma & Zhang & Akiyama & Wang & Song 2020, p. 760.) For high pressure applications, the concentration of dissolved hydrogen (C_H) can be calculated as per Sievert's law:

$$C_H = S\sqrt{P_{H_2}} \tag{1}$$

where S is the solubility constant (dependent on the alloy and temperature) and P_{H2} is the partial pressure of hydrogen (Li et al. 2020, p. 760).

Although it must be noted that in practice the concentration of dissolved hydrogen is almost invariably higher than the value calculated with Sievert's law due to the high number of hydrogen traps in steel. These can be divided into reversible and irreversible trapping sites, depending on the energy required to dissolve the hydrogen particles from the steel, also known as binding energy, which unit is typically measured in unit of kJ/mol. Examples of

reversible trapping sites are dislocations, interstitial sites, lath and grain boundaries and coherent precipitates while inclusions, interfaces between different constituents such as ferrite/cementite, Fe_3O and Al_2O_3 and incoherent precipitates are considered irreversible. (Li et al. 2020, p. 761; Ugwu & Morgan & Ibrahim 2021, p. 2250.) The minimum value of binding energy for traps being irreversible is considered to be 60 kJ/mol, but this is also dependent on the type of trap site as well as alloy, as some alloying elements increase the trapping site formation (Goutam & Rostron & Garg & Panday 2018, p. 611).

The nature of possible strain also has an effect on the diffusion of hydrogen in a way that elastic strain increases hydrogen's diffusion susceptibility whereas plastic strain decreases it (Goutam et al. 2018, p. 611).

As Sievert's law demonstrated, the hydrogen's solubility in steels is dependent on the alloy. This observation is directly based on the fact that some metals are more subject to dissolving hydrogen than others. For example, γ-iron has a significantly higher heat of solution for hydrogen than chrome-alloyed austenitic stainless steels. In addition, different metals behave differently under changing temperatures; iron's hydrogen solubility for instance, almost invariably increases as the temperatures rise. Titanium on the other hand has lower solubility at higher temperatures. Moreover, the crystalline structure of the steel affects solubility. This can be noticed when comparing austenitic and ferritic stainless steels. The former's face-centered cubic crystalline structure contributes to its higher solubility compared to body-centered cubic crystalline structure of the ferritic stainless steel. (Nagumo 2016, pp. 1-4.)

Hydrogen can get in contact with steel in a liquid or gaseous phase, but once the bulk of the material absorbs the hydrogen, the original phase generally does not matter. Before the absorption process, the form of hydrogen, load level, and strength of the steel define its effect on the steel. The types of steel most likely to suffer from hydrogen embrittlement are typically the ones under high loads, hardened or cold-rolled, while, for instance, the molecular form of hydrogen usually does not cause embrittlement at all but causes blistering instead. (Cheng 2013, pp. 21-22.)

2.2 Lattice location of hydrogen

The precise location of hydrogen atom in the lattice is challenging to determine due to its small solubility and high diffusivity, but in an ideal crystal, hydrogen atoms are typically located in BCC tetrahedral or FCC octahedral interstitial sites (Nagumo 2016, p. 5; Li et al. 2020, pp. 760-761). This general guideline also applies to iron, whereas for instance in nickel, the atoms are located primarily only in octahedral sites (Gavriljuk & Shyvaniuk & Teus 2022, pp. 10-12).

2.3 Crystallographic defects

There are always some types of defects, such as vacancies, dislocations and grain boundaries in lattice, and hydrogen will interact with them, affecting the material's mechanical properties (Nagumo 2016, p. 35; Gavriljuk et al. 2022, p. 45). This chapter will present the most relevant and notable types of defects when the effect of hydrogen on steel is considered.

2.3.1 Vacancies

Vacancies in itself have an effect on hydrogen and they work as traps for hydrogen advancing the diffusion. Moreover, hydrogen affects the vacancies resulting in an increase in the number of defects in metal and leading to increased plasticity. Hydrogen accumulation can also increase the local stress in lattice and thus contribute to vacancy formation. (Hayward & Fu 2013, p. 4.)

2.3.2 Dislocations

Hydrogen and its interactions with dislocations are the most usual explanation behind the change in metals' mechanical properties. The moving dislocations act as a route for hydrogen to advance towards the grain boundaries. This has also been noted as a reasoning behind the increased fatigue crack growth rates whenever hydrogen is present. Dislocations, caused by plastic deformation, can also lead to other lattice defects, such as vacancies and interstitial atoms. (Nagumo 2016, p. 35; Gavriljuk 2022, p. 121.)

2.3.3 Grain boundaries

Typical points of occurrence for hydrogen are grain boundaries since they are generally considered susceptible to increased diffusion in metals, but the level of diffusion through the grain boundary is not standard but depends on the material. Depending on the type of interface, the binding energies of hydrogen in them will also vary. Although, hydrogen in grain boundaries does not automatically mean the risk of intergranular fracture is increased, the consensus is that it might contribute to hydrogen embrittlement. (Gavriljuk 2022, p. 125; Nagumo 2016, pp. 59-60.)

2.4 Hydrogen theories

When hydrogen-induced failure modes, such as hydrogen embrittlement and hydrogen-induced cracking are considered, the mechanisms behind the hydrogen degradation phenomena are not always unambiguous as not every theory is suitable for every situation. Chapters 2.4.1-2.4.5 will present different theories that can be used to explain the effect of hydrogen on steel. However, it should be noted that some theories are considered more credible than others, and some might even be based on nothing but retrospective observations of samples.

2.4.1 Hydrogen pressure theory

According to the hydrogen pressure theory, the individual hydrogen atoms diffuse into the bulk of the steel and locate at the imperfections such as grain boundaries, interstitials and voids in the metal and then combine into hydrogen molecules. As time passes, the hydrogen atoms close to the imperfections keep moving closer to them, causing increased hydrogen pressure inside the imperfections, leading to crack nucleation and, eventually crack propagation when the material’s strength limit is exceeded. This theory can be used to explain the hydrogen embrittlement and hydrogen-induced cracking. (Li et al. 2020, p. 764; Mohtadi-Bonab & Pourazizi & Szpunar 2020, p. 23124.)

2.4.2 Hydrogen-induced phase transformation

Hydrogen-induced phase transformation (HIPT) theory is based on the statement that some metals when exposed to hydrogen are prone to formation of brittle hydrides. The fracture failure that occurs in metals containing these hydrides begins with hydrogen first accumulating at the tip of the crack, then proceeding to hydrogen and metal unification and crack expanding to the formed hydride. The crack formation stops at the edge of the hydride, but repeated occurrences lead to crack propagation. Depending on the amount of hydrogen in the alloy, the hydrogen's and metal's unification behavior varies. When the hydrogen content is low, hydrides form either spontaneously or because of stress. With high contents of hydrogen, hydrides are formed purely spontaneously. HIPT is considered to be a one suitable theory for explaining hydrogen embrittlement in metals. (Li et al. 2020, p. 764-765.)

2.4.3 Hydrogen-enhanced localized plasticity mechanism

Hydrogen-enhanced localized plasticity mechanism (HELP) is closely related to the plasticity of the metal, and it has been linked with hydrogen embrittlement and hydrogen-induced cracking. The theory behind the mechanism is that hydrogen atoms diffused into the bulk make it easier for the dislocations in the crystal structure to grow and move thus requiring lower stresses for dislocation movement and increasing the plasticity of the material. This, in turn, causes an accumulation of dislocations, thus causing an increased risk of failure in the metal. When HELP is considered, the microstructure of steel, the concentration of hydrogen, distribution of precipitates and inclusions, and stress intensity have a great effect. (Li et al. 2020, p. 765; Mohtadi-Bonab et al. 2020, p. 23125.)

2.4.4 Hydrogen-enhanced decohesion

The main argument behind the hydrogen-enhanced decohesion mechanism (HEDE) is that the presence of hydrogen in metals increases the possibility of atom separation. This theory states that hydrogen atoms take advantage of imperfections such as grain boundaries, precipitates, and interstitials in steel, diffusing through them and thus reducing the strength of the atomic bindings. Consequently, this leads to an occurrence of slip, which is a

displacement of a part of the crystalline structure. It must also be noted that even though the HEDE mechanism has been confirmed theoretically to explain hydrogen embrittlement and hydrogen-induced cracking, at least for now, there has not been a successful practical study to confirm the theory to be correct. (Li et al. 2020 p. 765; Mohtadi-Bonab et al. 2020, p. 23124.)

2.4.5 Hydrogen-enhanced strain induced vacancies

According to Nagumo (2004, p. 949), "The presence of hydrogen enhanced the increase in strain induced trapping sites and reduced ductile crack growth resistance." This statement explains the principle behind the hydrogen-enhanced strain induced vacancies (HESIV). As a results, the increased number of vacancies increases the risk of failure in metals. HESIV can be used for explaining hydrogen embrittlement in metals, especially the one of reversible nature. (Li et al. 2020, pp. 764-767.)

2.5 Hydrogen embrittlement

Hydrogen embrittlement is a phenomenon affecting several metallic materials. Even the carbon steel pipes meeting the API requirements for oil and gas use are not immune to it. (Mahajan & Tan & Venkatesh & Kileti & Clayton 2022, p. 12.) Susceptibility to hydrogen embrittlement is not standard for all steels and some alloys and microstructures are considerably more prone to it than others. For example, austenitic steels, aluminum, copper and nickel alloys are comparatively resistant to hydrogen embrittlement, whereas martensitic high-strength steels are susceptible to hydrogen embrittlement. (Li et al. 2020, pp. 759-760.) When austenitic steel is examined further, its resistance to martensitic transformation has a great effect when hydrogen embrittlement is considered. Heat treatments done to the steel also affect the hydrogen embrittlement susceptibility. (Nagumo 2016, pp. 188-190.) Steels under relatively high loads also have an increased risk of hydrogen embrittlement (Cheng 2013, p. 22). Ferritic steels with yield strengths under 750 MPa are an example of something in between the aforementioned instances (Shoji & Raja 2011, p. 92). In general, when the pressure of hydrogen increases and strain rates decrease, the risk of hydrogen embrittlement becomes more feasible (Cheng 2013, p. 22). When temperature is considered, ambient

temperature is a condition where hydrogen embrittlement is most likely to happen (Ciaraldi 1992, p. 45). Additionally, the BCC crystalline structure of the steels makes the effect of hydrogen embrittlement more damaging since it allows for greater mobility of hydrogen atoms (Gavriljuk et al. 2022, p. 91). Due to the hydrogen embrittlement's negative effect on materials' mechanical properties (mostly their ductility, but also tensile and fatigue strength) hydrogen embrittlement must be taken into consideration whenever hydrogen is present. Typical of failures, the conditions do not even have to be particularly demanding, but a brittle fracture can occur under light loads. (Li et al. 2020, p. 759.)

There is no clear all-embracing theory to explain the principle of hydrogen embrittlement, but generally, hydrogen embrittlement can be classified as reversible and irreversible. In reversible hydrogen embrittlement, hydrogen atoms gravitate toward the weak spots in the metal and slowly start inducing a fracture. This type of hydrogen embrittlement can be interrupted with a special hydrogen removal treatment. In the irreversible hydrogen embrittlement, two or more hydrogen atoms are connected into a molecule, which then locate at a potential imperfection, leading to a localized high hydrogen gas pressure and hydrogen-induced cracking. There are several theories that aim to explain the mechanism of hydrogen embrittlement, all of which are not suitable for every type of hydrogen embrittlement and cannot explain every single part of the process. Hydrogen pressure theory, hydrogen-induced phase transformation, hydrogen-enhanced localized plasticity mechanism, hydrogen-enhanced decohesion mechanisms and hydrogen-enhanced strain induced vacancies mechanism were presented in chapters 2.4.1-2.4.5. It must also be noted that the theory behind the latter three of the aforementioned mechanisms is based purely on the retrospective observations of used samples. (Li et al. 2020, pp. 764-768.)

2.6 Hydrogen-induced cracking

Hydrogen-induced cracking (HIC) is a failure mechanism associated especially with pipelines and concerns carbon and low alloy steels. The microstructure of the steel also has a notable effect on its tendency to suffer from HIC; for example, acicular ferrite and ultra-fine ferrite are considered the most HIC-resistant microstructure of the steel, while bainitic ferrite is comparably more susceptible. Especially carbon is a type of alloying element that encourages to create a bainitic or martensitic microstructure in steel, and both of these

features can increase the risk of cracking. In general, existing defects and other heterogeneous features increase the risk of HIC even further. (Goutam et al. 2018, pp. 609-613; Cheng 2013, p. 23.) Furthermore, the increased strength of steel also increases its tendency to suffer from HIC, which has to be considered while adding alloying elements since many of them have an effect on the strength of the steel in addition to other properties.

For piping steels, examples of typical alloying elements in addition to carbon are chromium, copper, manganese, molybdenum, nickel, titanium, and vanadium, which all have different effects on the microstructure of the steel and, thus the HIC susceptibility. For instance, the presence of carbon and manganese usually results in hard bainitic or martensitic microstructures, and, especially, the manganese's susceptibility to segregation increases the risk of HIC. Also, chromium and molybdenum also have a drastic effect on the microstructure; chromium addition reduces the HIC tendency, while molybdenum increases the absorption of hydrogen, and thus, the HIC susceptibility is higher. It could be concluded that chromium and molybdenum have opposite effects on the material when viewed from the hydrogen's point of view. Further, for example copper tends to increase the HIC resistance of the steel by creating traps for hydrogen and also reduce the hydrogen diffusion by forming a protective layer on the surface of the steel. The effect of titanium in an alloy depends on the size of the titanium particles where coarse particles will act as a suitable spot for cracking to occur whereas finer ones typically reduce the hydrogen segregation in the material. Despite the significant effects of alloying elements in steel when HIC is considered, nonmetallic inclusions are still regarded as more prominent factors contributing to HIC. (Goutam et al. 2018, pp. 613-617; Popov 2015, p. 345.)

Typically for HIC occurrence, the yield strength of the steel does not need even to be exceeded, and external stresses can be relatively low. Instead, steel's contact with hydrogen is more long-term in nature which allows the hydrogen molecules to absorb into the bulk and create internal pressure. (Goutam et al. 2018, p. 609.) Cracking patterns formed as a consequence of hydrogen are almost invariably sharp and singular instead of branching, as found in stress corrosion cracking, for example. Cracks are usually located either on the surface of the material or in the bulk at the defect location. (Cheng 2013, p. 23; Goutam et al. 2018, p. 609.) The location and the length of the crack can also indicate its source. Typically, the cracks inside the bulk of the material are related to inclusions which are

heavily connected to HIC in general, while the cracks generated near the surface of the material are not. (Goutam et al. 2018, p. 612.)

As with hydrogen embrittlement, there is no single comprehensive theory to explain every single HIC occurrence, and the mechanics behind it are not even completely understood. However, there are several theories that are considered to be reliable in explaining HIC. These are internal pressure theory, hydrogen enhanced decohesion and hydrogen enhanced localized plasticity, which are explained in more detail in chapters 2.4.1, 2.4.3 & 2.4.4. (Mohtadi-Bonab et al. 2020, p. 23124.)

2.7 Stress corrosion cracking

Stress corrosion cracking (SCC) is a type of mechanical failure mode caused by unfavorable conditions, leading to a growth of crack formation in a corrosive environment. One example of a favorable condition for a SCC to occur is hydrogen embrittlement of high-strength steels. However, it has to be noted that hydrogen can cause cracking even in the absence of a corrosive environment. (Cheng 2013, pp. 7-10 & 20.) Although stress corrosion cracking is mostly an issue with alloy steels, it also has to be considered even with non-alloy steels (Jones & Ricker 1992, p. 2).

In addition to environmental requirements, the tensile stress has to be adequate for SCC, and not all materials are equally susceptible to SCC either. There is no precise limit for tensile stress for SCC to occur, but typically, it does not even have to exceed the yield strength of the metal and can be rather low since there are usually local stress concentration points at defects of the surface of the material. (Cheng 2013, pp. 7-10 & 20.) Another aspect affecting the susceptibility to SCC is hydrogen partial pressure, where higher pressure leads to a higher risk of failure; this aspect is especially true for high-strength steels. Further, when temperature is considered, the high-risk temperature range starts from as low as -46 ˚C and can be as high as 120 ˚C, with ambient temperature being the most SCC-sensitive condition. (Ciaraldi 1992, pp. 47-48.)

The phenomenon of SCC is slow in nature and typically considered to consist of three phases: crack initiation, steady-state crack propagation, and failure. When all the other conditions are favorable, surface defects are susceptible areas for crack initiation to occur.

The subsequent crack propagation can follow the lines of grain boundaries or entirely cross them while being rather unnoticeable in the beginning but expanding as the crack propagation proceeds and possibly forming prominent deformations in the steel. Shared factors for both intergranular and transgranular SCC are, for example, temperature, pH, oxygen concentration and chemistry of the crack tip. (Jones & Ricker 1992, pp. 3-17.)

The mechanics of crack propagation can be generally divided into dissolution-based and mechanical fracture-based models. When the dissolution model is considered, several theories have explained its concept, including the film-rupture model being noted as the most credible. According to the film-rupture theory, crack, rupture, and the protective film of the surface are torn by the stress affecting the steel, which then subsequently ends up exposing the easily dissolving bare metal and thus advancing the crack propagation. When it comes to the mechanical fracture-based models, there have been several suggestions for a theory explaining the phenomenon. Two main categories for mechanical fracture models are ductile crack-extension and brittle crack-extension. Ductile model theories include the adsorption-enhanced plasticity model and the corrosion tunneling model. The adsorption-enhanced plasticity model is based on the statement that fracture is caused by the environment via the adsorption of outside elements into the surface of steel. An example of a phenomenon following this theory is hydrogen embrittlement. The corrosion tunneling model is a mechanism based on the corrosion tunnel formation in the steel, which then expands in size and subsequently causes ductile deformation and fracture one after the other. Brittle crack-extension theories are further divided into the tarnish-rupture model and the film-induced cleavage model. The tarnish-rupture model states that a brittle film forms on the surface of a metal, which is prone to react with the environment when the film fractures. This reaction creates a new film on the surface of the metal, and the crack propagation continues by switching between film creation and fracture. The existence of a thin film on the surface of a metal also acts as a basis for the film-induced cleavage model. This theory states that a brittle fracture first develops in the film of a metal and then quickly proceeds to the ductile bulk of the steel. The crack propagation will eventually stop, but a new crack will initiate, and the process starts all over again. The prerequisite for this model is a sharply shaped crack and fast crack propagation. (Jones & Ricker 1992, pp. 32-35.)

2.8 Hydrogen attack

Hydrogen attack is a phenomenon occurring at high temperatures of over 200 ˚C. In addition to temperature, parameters affecting the hydrogen attack are partial pressure of hydrogen, stress levels, exposure time, and microstructure of steel. Different types of treatments can also alter the microstructure of the steel and thus have an effect on hydrogen attack susceptibility. Even a slight increase in temperature, – for example from 225 ˚C to 250 ˚C, – usually causes significantly faster deterioration when hydrogen attack is considered. The same principle applies to pressure also, although not to the same extent. The minimum required pressure for hydrogen attack is considered to be around 0,7 MPa. While the presence of stress is not a limiting factor when the occurrence of hydrogen attack is considered, it still creates favorable conditions for the phenomenon, increasing the decarburization, that is considered to be a part of the hydrogen attack. (Poorhaydari 2021, pp. 7883-7903.) Carbon steels are particularly susceptible to hydrogen atoms reacting chemically with carbon, forming methane gas (Cheng 2013, p. 23; Kot 2001). These methane molecules get blocked inside the steel, thus advancing crack and fissure formation at the grain boundaries due to the increased number of defects in the microstructure of the steel. While not being completely immune, an example of a hydrogen attack-resistant steel is austenitic stainless steel, while martensite/bainite structure should be avoided. Fine grain size also increases the steel's ability to resist hydrogen attack. (Poorhaydari 2021, p. 7886.) The presence of some type of carbide-forming alloying elements in steel, such as chromium, molybdenum, or titanium, also reduces the risk of hydrogen attack since they act as carbide stabilizers (with the exception of molybdenum which affects the creep strength of the steel also supporting the steel's resistance to hydrogen attack). Another useful heat treatment technique in this regard is annealing, which is suitable, at least for Cr-Mo steels. (Poorhaydari 2021, pp. 7880-7886; Kot 2001.)

When a hydrogen attack first occurs, and hydrogen diffuses into the steel in favorable conditions, its mechanical properties do not deteriorate immediately; rather, only notably small methane bubbles are formed during the initial stages of the attack. If the hydrogen attack does not exceed beyond this first phase, it could still be reversed by annealing. However, if the phenomenon proceeds further, the mechanical properties of the steel start to

deteriorate at an increasing rate, and the damage is irreversible in nature while eventually evening out to small rates of deterioration. (Poorhaydari 2021, p. 7881.)

Apart from minor swelling, the damage caused by a hydrogen attack causes is purely internal and cannot be detected without more thorough testing methods. Typically, the damage caused by hydrogen attack is divided into two types, and the one that occurs depends on the conditions. Relatively low temperature and high hydrogen pressure favors internal decarburization and fissuring, which is also the most typical type of hydrogen attack to occur and is rather difficult to detect, which makes it especially dangerous. The temperature limit for internal decarburization is considered to be around 600 ˚C. With internal decarburization, the hydrogen diffuses into the bulk reacting with the carbon in the steel, generating localized high internal pressure, which leads to cracking. Fissuring along grain boundaries occurs at the same time. Whereas when the temperature is high and hydrogen pressure is low surface decarburization occurs, where carbon diffuses into the surface of the steel and forms methane and carbon dioxide gas. (Poorhaydari 2021, pp. 7882-7884.)

2.9 Hydrogen compared to natural gas

When planning to change the flowing substance in the pipeline for something the pipe was not originally designed for, the possible differences between the substances have to be considered. This is also true for hydrogen and natural gas, even though they also share some attributes. First of all, while both of them are extremely flammable, the explosion caused by hydrogen is even more intense than natural gas. Related to this, it has been studied that methane-hydrogen mixtures where the percentage of hydrogen is over 40 % would have an increased risk of sudden explosions and harmful overpressures, while mixtures with lower amounts of hydrogen would be no different from pure methane gas when flammability is considered. Also, due to the fact that the size of the hydrogen molecule is smaller, and it is extremely lightweight compared to natural gas, the risk of leakage increases significantly. Furthermore, the addition of hydrogen always enables the possibility of hydrogen embrittlement and other hydrogen-induced failure modes, which the steel selected originally for the pipeline was not designed to withstand. (Mahajan et al. 2022, pp. 10-11.)

All these differences between natural gas and hydrogen lead to a requirement for stricter leakage detection, and the same methods utilized with natural gas might not be applicable

for hydrogen. For example, hydrogen molecules are much more eager to diffuse into the air than natural gas, resulting in lower readings than natural gas with similar leakage levels. (Ferreira & Fonseca & Adame & Bundaleski & Robinson & Teodoro 2024, p. 1091.)

3 Methodology

This section of the thesis contains the actual research part of the work, presenting the methods used to execute the pipeline analysis. It will first introduce a common pipeline steel grade which will be used as an example for the analysis. The exact composition of the alloy will be presented, as well as dimensions, environmental factors, and other significant elements that would realistically represent an existing natural gas pipeline.

The first step will be to gather the stress intensity factor range at the crack tip which will be acquired using FE-analysis, whose model and its setup will be presented. The results will then be used to analyze the piping material's suitability for hydrogen.

The purpose of the analysis is to implement crack growth rate plots of the pipeline crack in the presence of natural gas and hydrogen, compare the two mediums and evaluate the pipeline's suitability for transporting hydrogen instead of natural gas. Unlike hydrogen, natural gas does not have an effect on the crack growth rate, which means that the crack growth rate graph of natural gas can be compared to the situation without any specific medium.

3.1 Analysis specifications

API 5L Grade X52 steel was chosen as the material to be used in calculations due to it being a very typical choice for natural gas pipelines. Detailed specifications of the X52 grade as per API Specification 5L are presented in Table 1.

Table 1. Chemical composition of X52 PSL 1 (Api Specification 5L 2018, p. 29).

C	**Mn**	**P**	**S**	**V**	**Nb**	**Ti**
Max (%)	**Max (%)**	**Max (%)**	**Max (%)**	**Max (%)**	**Max (%)**	**Max (%)**
0,28 (seamless pipe)/0,26 (welded pipe)	1,40	0,030	0,030	V + Nb + Ti ≤ 0,15	V + Nb + Ti ≤ 0,15	V + Nb + Ti ≤ 0,15

When it comes to the calculation, the dimensions of the section of a pipeline and other essential parameters were chosen to represent an actual natural gas pipeline. This information is shown in Table 2. The parameters were assumed to stay constant between both mediums: natural gas and hydrogen.

Table 2. Calculation parameters.

Material	API 5L Grade X52
Pipe nominal size	DN400
Wall thickness	6,35 mm
Pipe section length	700 mm

The selected DN400 nominal size represents a typical size for a branch in a pipeline, used to transport natural gas to the final destination, such as a processing facility. The pipeline section of this size can typically have a length of over 10 kilometers, but for relevancy a shorter section length of 700 mm was chosen.

3.2 FE-model setup

The FEA was carried out using 2024 R1 version of the Ansys Mechanical solver. The model and its setup, including the loads, constraints, crack dimensions, mesh, and other parameters, will be presented in this chapter.

3.2.1 3D-model

The 3D-model of the pipeline section was done using the DesignModeler modeling tool found in Ansys. The diameter dimensions were chosen to represent the size of a DN400 pipe, and the length was limited, according to the dimensions shown in Table 2. The exact dimensions of the 3D-model are presented in Table 3. Figures 1 and 2 showcase the isometric view, and the cross-section view of the 3D-model respectively.

Table 3. Dimensions of the 3D-model.

Property	Value
Outside diameter (mm)	406,4
Inside diameter (mm)	393,7
Section length (mm)	700

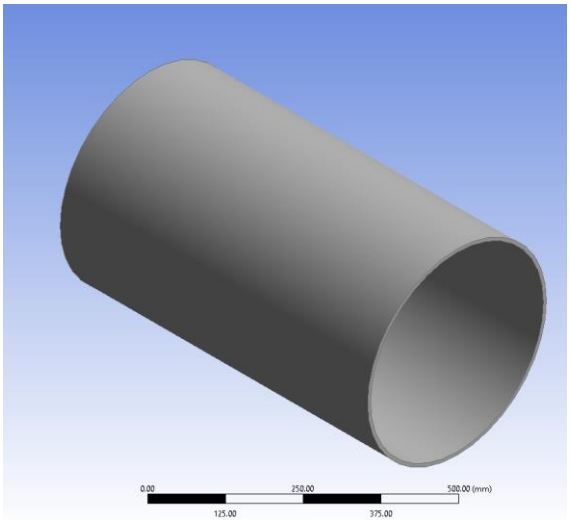

Figure 1. Isometric view of the 3D-model of the pipeline section.

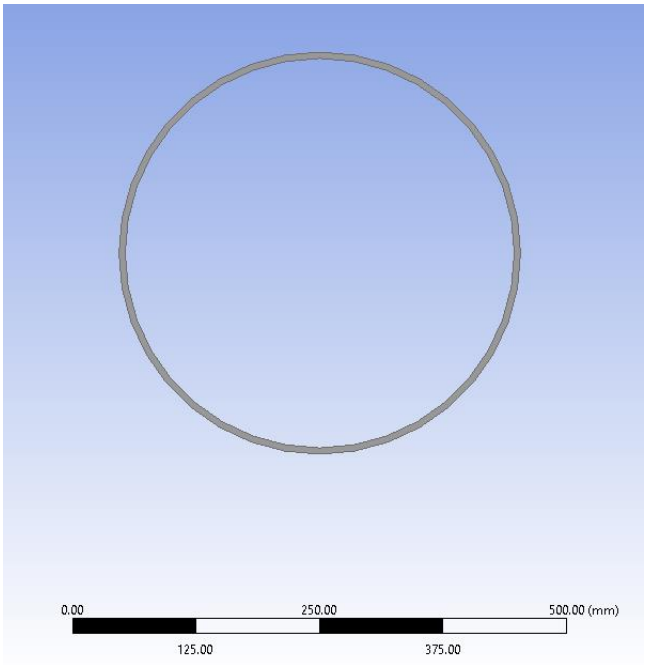

Figure 2. Cross-section view of the 3D-model of the pipeline.

3.2.2 Material parameters

The material properties used for the FEA were chosen to be equivalent to the X52 grade steel commonly used in pipelines. The material properties relevant to the FEA are shown in Table 4. It must be noted that while Young's modulus, Poisson's ratio, yield strength and ultimate strength have generic values for X52 grade steel and are readily available, Paris' Law material constants C and m on the other hand have variation inside the literature but the values used in this analysis were the ones mentioned in Darcis & Treinen & McColskey (2009, pp. 6-7), which were derived using the methods of ASTM E 647-05 standard.

Table 4. FEA material properties.

Property	Value
Young's modulus (GPa)	200
Poisson's ratio	0,3
Yield strength (MPa)	360
Ultimate strength (MPa)	460
Paris' Law material constant C ($MPa \times mm^{1/2}$)	$1{,}22 \times 10^{-14}$
Paris' Law material constant m	3,49

3.2.3 Loads

The only load used in the analysis was the pressure applied toward the inner surface of the model, which was equivalent to the pressure load caused by the medium inside the pipeline; Figure 3 shows the loading area colored in red. The load was initially set up with a static value. Then, using the Fatigue Tool in Ansys Mechanical, the loading ratio and frequency were set, mimicking a fluctuating pressure load inside the pipeline; Table 5 displays the properties of the load given.

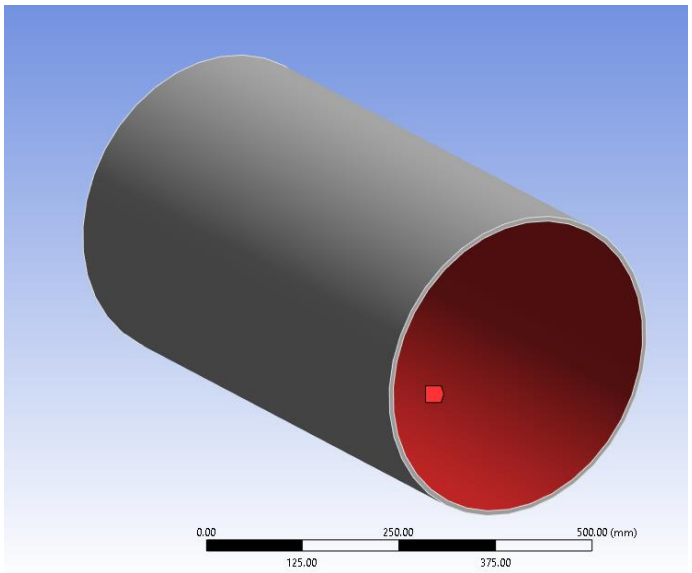

Figure 3. 3D-model with loading area highlighted.

Table 5. Load properties of the analysis.

Property	Value
Pressure (MPa)	4
Loading ratio	0,8
Frequency (Hz)	0,033

The selected pressure for the simulation was chosen since there are examples of existing natural gas pipelines of the same size and material, and the maximum operating pressure is 5,4 MPa. Loading ratio and frequency were set to represent one scenario, although, in typical conditions, the frequency can be considered to be lower, resulting in more stable pressure inside the pipeline.

3.2.4 Constraints

Since the purpose of the analysis was to examine the stress intensity factor values at the crack tip, it could be assumed that the pipeline itself around the crack stays still. Therefore, the model of the pipeline section was constrained using fixed supports in the planes at both ends of the model. This boundary condition prevented all the translations and rotations in every axis. Figure 4 displays the plane used for the placement of the fixed support, which is marked in blue. The opposite side of the model is constrained in a similar way.

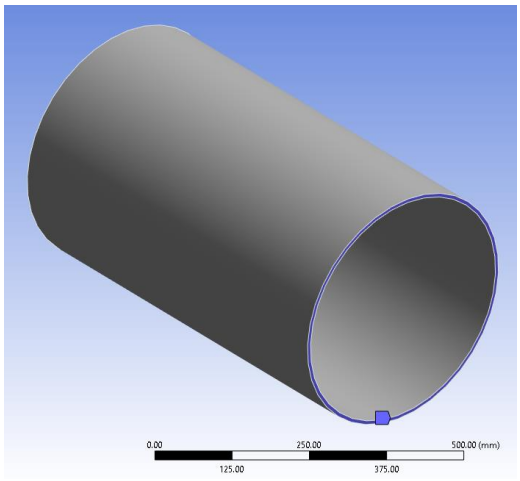

Figure 4. 3D-model with the constraint highlighted.

3.2.5 Crack properties

The crack used for the analysis was made with the Fracture tool found in Ansys Mechanical. The crack shape was chosen to be semi-elliptical with a major radius of 18 mm and a minor radius of 3 mm. It was placed in the inner surface of the pipe, placing the center point of the crack in the exact middle point of the pipe in the longitudinal direction. Figure 5 shows the location of the crack in the isometric view, and Figure 6 displays the view looking down at the Y-axis perpendicular to the crack.

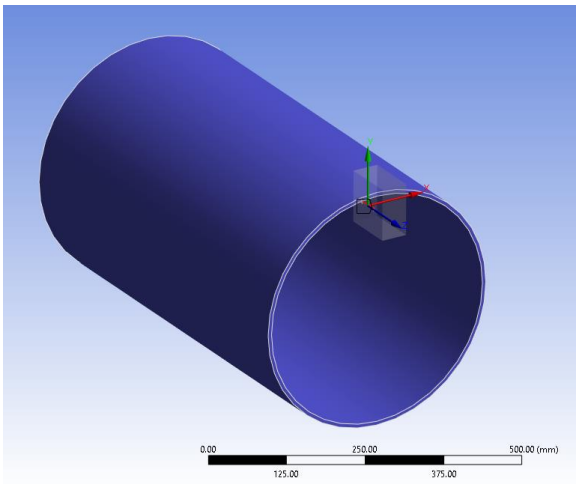

Figure 5. Isometric view of the 3D-model and the crack location.

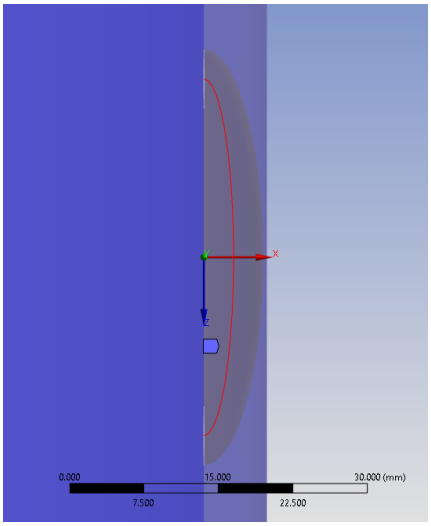

Figure 6. Top view of the crack.

In addition to placing the crack geometry to the model, Ansys' SMART Crack Growth was used. This tool enables automatic remeshing during a simulation to make results more accurate.

3.2.6 Mesh

The model was first meshed using a general element size of 40,0 mm. Additionally, the mesh around the crack was made significantly denser due to it being the area of interest in the model. Figure 7 shows the general view of the model with the meshing, while Tables 6 and 7 present the more precise meshing setup for the general mesh and the crack mesh, respectively. It should be noted that a mesh method of the model had to be set to "Tetrahedrons" in order for the SMART Crack Growth feature to work.

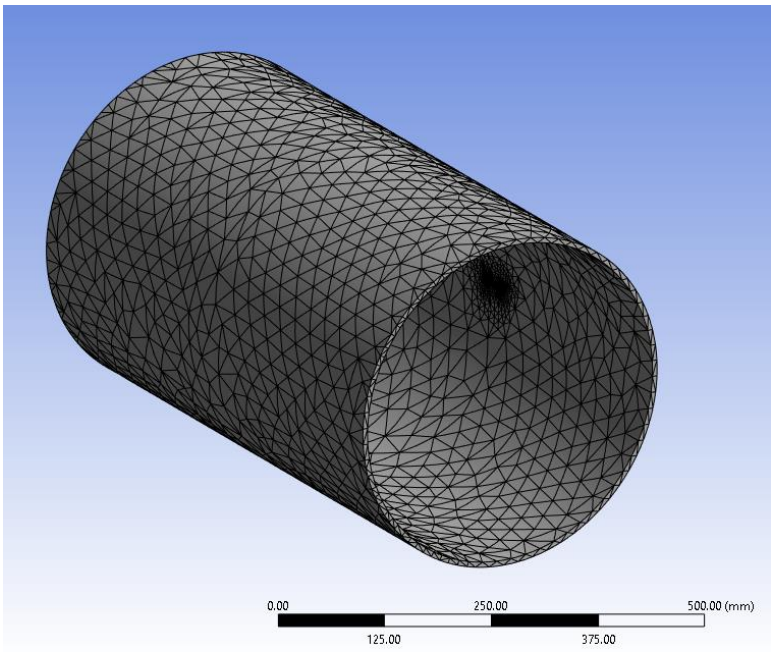

Figure 7. General view of the meshing of the model.

Table 6. Mesh information of the model (Ansys Mechanical 2024 R1).

Property	Value
Definition	
Method	Tetrahedrons
Algorithm	Patch Conforming
Element Order	Quadratic
Advanced Improve Options	
Aggressive Thin Face Collapse	Program Controlled
Automatic Node Movement	Program Controlled

Table 7. Mesh information of the crack (Ansys Mechanical 2024 R1).

Property	Value
Mesh Method	Tetrahedrons
Largest Contour Radius	3 mm
Growth Rate	Default (1.2)
Front Element Size	Default (0.55778 mm)
Mesh Contours	4
Solution Contours	Match Mesh Contours

3.2.7 Analysis settings

The number of steps for the analysis was set for 100 and length of the step as 1 second. Regarding the crack growth criteria, the choice must be made between J-Integral or SIFS since both of them cannot be solved with SMART Crack Growth tool. The SIFS was chosen for the analysis.

3.3 Fatigue crack growth rate plot

This chapter will present the methods used to form a fatigue crack growth rate plots with the results of the FEA. The plot for natural gas can be formed rather easily with a well-known

equation, but for hydrogen, this cannot be utilized, and a more specialized crack growth law is required.

3.3.1 Natural gas

The rate of the fatigue crack growth can be solved with Paris' law which is as follows (Pugno, N., Ciavarella, M., Cornetti, P. & Carpinteri, A. 2006, p. 1338):

$$\frac{da}{dN} = C(\Delta K)^m \tag{2}$$

where *da/dN* represents the fatigue growth in relation to load cycles, *C* and *m* are material coefficients, and *ΔK* is the SIF (stress intensity factor) range. The results are typically plotted with *da/dN* on the y-axis and *ΔK* on the x-axis.

The aforementioned equation 2 can be utilized when there are no additional factors affecting the crack growth, such as hydrogen, which increases the crack growth tendency. Since methane, the main component of natural gas does not have an effect on the crack growth rate, and the share of other components is significantly smaller (Juan & Guo & Xing & Gao & Hua 2024, p. 636), Paris' law was used when estimating the crack growth in natural gas environments.

Accordingly, Paris' law was used to form a fatigue crack growth rate plot for natural gas, using the SIF range from the results of the FEA. Paris' Law material constants C and *m* play a crucial role in the results, and the same values from the FEA were used (Table 4).

3.3.2 Hydrogen

As the general form of Paris' Law is not reliable for estimating the crack growth rate with hydrogen's effect, a more specific equation was used. The literature has presented several different options for this, but the DVGW G 464 standard-based equation is used here. The crack growth law has two different forms depending on the *ΔK* values. The equations are as follows (Oesterlin & Fischer & Michler 2024, p. 6):

$$\frac{da}{dN} = 4{,}4 * 10^{-13}(1+3R)\Delta K^{7}\sqrt{p_{H_2}} \quad (3)$$

when:

$$\Delta K \leq [3.6667 * 10^{-6}\sqrt{p_{H_2}}]^{-0{,}25}\ MPa\sqrt{m} \quad (4)$$

and:

$$\frac{da}{dN} = 1{,}2 * 10^{-7}(1+3R)\Delta K^{3} \quad (5)$$

when:

$$\Delta K \geq [3.6667 * 10^{-6}\sqrt{p_{H_2}}]^{-0{,}25}\ MPa\sqrt{m} \quad (6)$$

In the equations 3, 4, 5, and 6, *da/dN* represents the fatigue growth in relation to load cycles, *R* is the loading ratio, *ΔK* is the SIF range, and p_{H_2} is the pressure of the hydrogen in bars.

As with the general form of Paris' law when calculating the crack growth rate with natural gas as a medium, SIF values from the FEA results were used when plotting the results with hydrogen. The value for the loading ratio was the same as that used in the FEA (Table 5). Hydrogen pressure p_{H_2} was assumed to be equal to the pressure of natural gas in the FEA (Table 5) with units converted to bars from MPa.

4 Results

This chapter will present the results of the FEA implemented with the methods mentioned in Chapter 3. Moreover, the resulting stress intensity factor range will be used to form a fatigue crack growth plot for the X52 steel with natural gas as a medium. An equivalent plot with the presence of hydrogen will also be formed.

4.1 FEA results

This chapter will contain the SIF values from the FEA done as described in Chapter 3.

The plotted values of SIF in relation to time are presented in Figure 8.

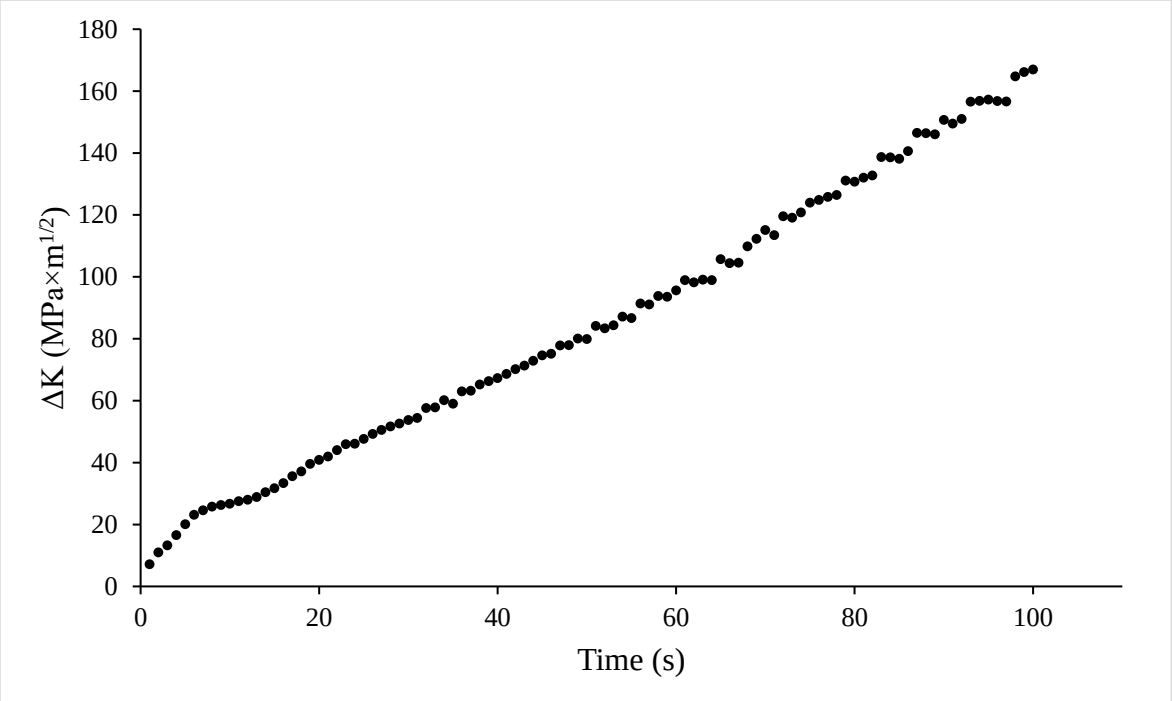

Figure 8. Stress intensity factor range in relation to time.

As can be seen from Figure 8, with the used loading, crack, and other properties, the SIF range values increase linearly and rather rapidly over time.

4.2 Fatigue crack growth rate with natural gas as a medium

This chapter will present the fatigue crack growth rate curve for X52 steel with natural gas as a medium, which can then be used as a basis for comparison with the equivalent curve of hydrogen used as a medium.

The fatigue crack growth rate curve was implemented as described in Chapter 3. The SIF range values used were those obtained with FEA, although it does not really matter for the crack growth plot since the results depend on Paris' law constants. The finished curve can be seen in Figure 9.

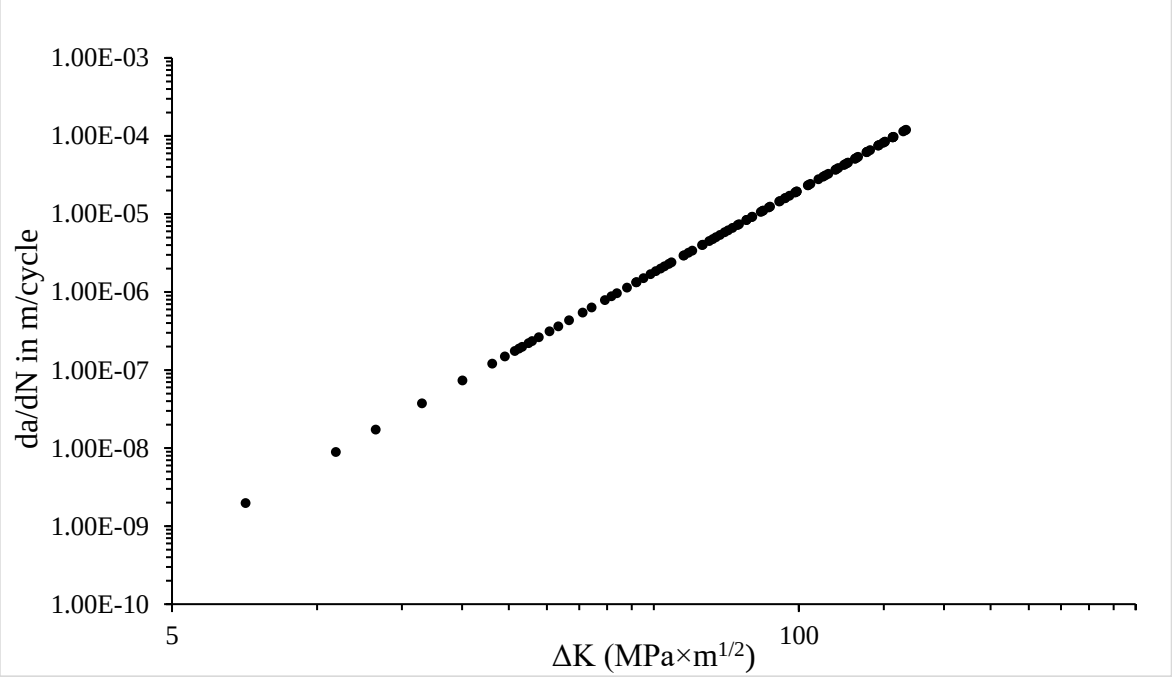

Figure 9. Fatigue crack growth rate of X52 steel in natural gas presented in log-log plot.

4.3 Fatigue crack growth rate with hydrogen as medium

This chapter will present the fatigue crack growth curve for X52 grade steel with hydrogen as the medium.

Similar to the fatigue crack growth curve with natural gas, the equivalent plot for hydrogen was formed as presented in Chapter 3. As the SIF range is mostly over the value defined in equation 4, equation 5 was used for calculating the crack growth rate. Figure 10 shows the fatigue crack growth rate in hydrogen.

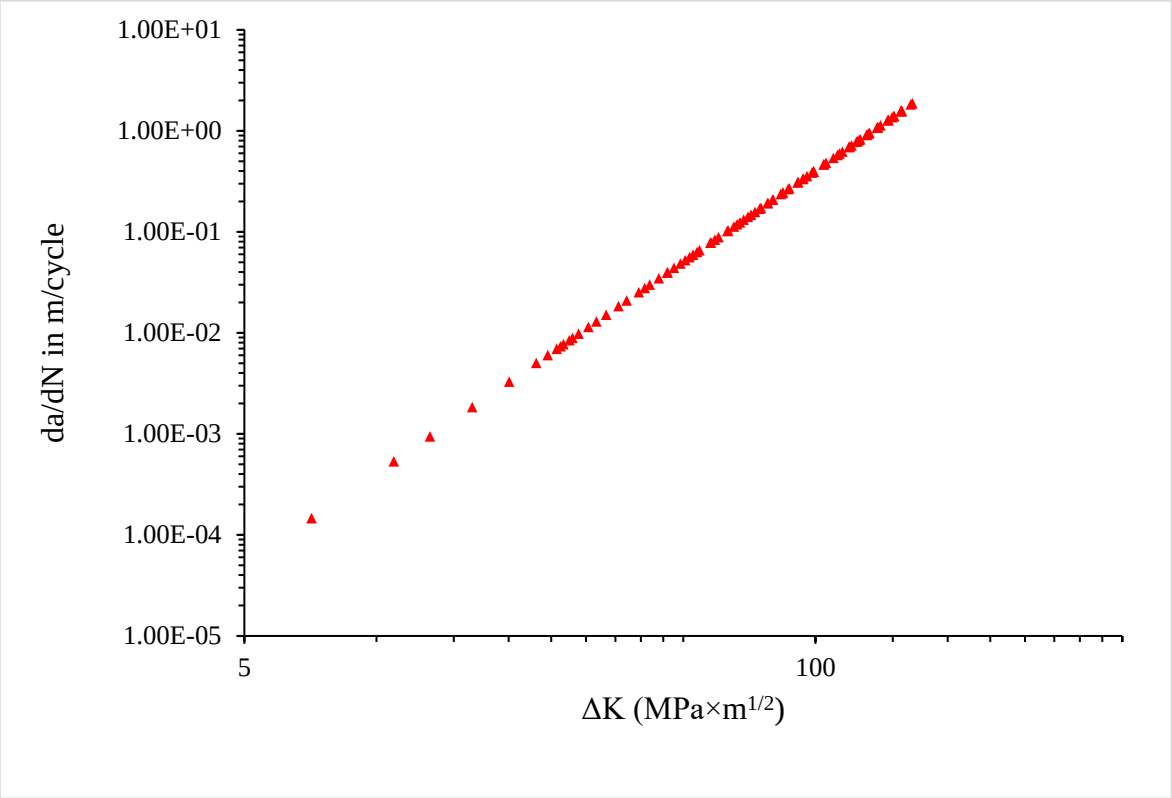

Figure 10. Fatigue crack growth rate of X52 steel in hydrogen presented in a log-log plot.

Figure 11 shows the fatigue crack growth rate curves for both natural gas and hydrogen in combined plot.

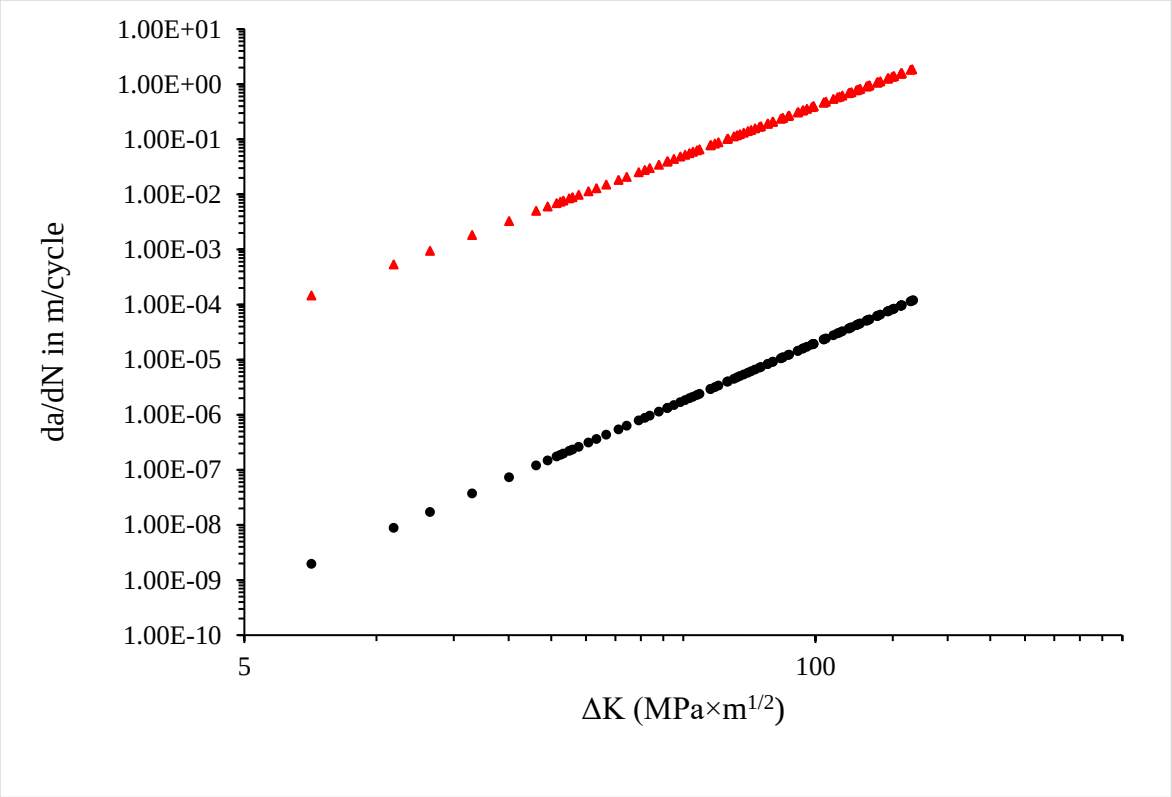

Figure 11. Combined plot for fatigue crack growth rate curves for natural gas (black) and hydrogen (red).

5 Discussion

This chapter will focus on discussing the results and evaluating their validity. First of all, it must be noted that while the pipe size and the material were chosen to represent the typical natural gas transmission pipeline, there are several different sizes used, with some being significantly smaller and some larger than the DN400 size used in this analysis and the results only represent that specific size. The same applies for the API 5L X52 steel grade chosen as the material. While X52 is a very common choice for natural gas transportation, grades such as X65 and X80, for example, are also used and the results might be considerably different from those.

Another factor affecting the results is the loading properties, which affect both FEA results and fatigue crack growth rate plots. The chosen pressure inside the pipeline was assumed to be similar between both mediums, and its value itself can be considered rather realistic for the size of the pipe used. The fluctuation of the pressure was required for the fatigue crack growth, so the loading ratio and frequency for the load were set. In normal conditions, the set frequency of 0,033 Hz means it takes roughly 30 seconds for the pressure to oscillate between the lowest and the highest pressure is rather low, and the pressure could be considered to be much more consistent in typical operating conditions. Also, the loading ratio was set to be relatively high. A lower value would result in a smaller degree of crack growth as can be seen from the equation used for the fatigue crack growth rate in hydrogen. The same equation also reveals that the pressure of hydrogen is not actually taken into account at all when calculating the crack growth rate. With lower SIF range values, hydrogen pressure should be included, which could affect the results.

On the other hand, the equation chosen for calculating the fatigue crack growth rate for hydrogen was based on one source, and there are also other options found in the literature that may lead to different results. Paris' law used for natural gas, being more general in nature, leads to more unambiguous results. However, it is noteworthy that Paris' law material constants for a specific material and conditions are not generic, but the values presented in the literature have variations. Consequently, using material constant values from different sources could have resulted in different outcomes of calculations.

The validity of the fatigue crack growth rate results can be analyzed by comparing them to the literature. Because natural gas does not have an effect on the fatigue crack growth rate, its plot can be compared to the one implemented in air, which is readily available in research papers. For example, in Oesterlin et al. (2024, p. 2301012), the fatigue growth rate data of X52 in ambient air was presented, which shows a similar linear curve with equivalent crack growth rates for corresponding SIF range values. The plot in the Darcis et al. (2009, p. 6) study also shows a similar crack growth rate/SIF range relation with crack growth rates, being with the same scientific notation multiplier when looking at any given SIF range value. Also, small variations in the multiplier before the scientific notation can be considered to be due to differences in Paris' law constants. Based on these research papers and various other easily available fatigue crack growth rate curves for X52 steel, it can be assumed that the fatigue crack growth rate curve in the natural gas environment presented in this master's thesis can be used for reliable comparison with similar plots in hydrogenous environments.

The interesting part is the crack growth rate with the presence of hydrogen and how it compares to natural gas with similar SIF range values. The equation used to estimate the crack growth rate in hydrogen was based on the literature and there were two options to be chosen from (equation 3 and equation 5), depending on the SIF range value. Since the SIF range values were constantly over the defining threshold for the equation apart from the very lowest values, the equation for the higher SIF range values was used throughout the calculations. When examining the resulting fatigue crack growth rate curve, it can be noted that *da/dN* values are greater than the ones found in literature all along the load range with corresponding SIF range values. There are considerably fewer reference points found in the literature compared to crack growth in natural gas, but for example, in Oesterlin et al. (2024, p. 2301012), the plot includes several fatigue crack growth curves in gaseous hydrogen. All of these are of the different order compared to the curve executed in this work. However, it must be considered that those plots are obtained through experimental results.

On the other hand, when studying the plots in Chandra, Thodla & Sosa (2023, p. 5) for reference, the results are slightly more similar, although not completely comparable, since the plots in that study were conducted with a mixture of hydrogen and natural gas instead of pure hydrogen but this favors the results of this thesis. Another example can be found in Somerday & Sofronis & Nibur & San Marchi & Kirchheim (2013, p. 6157), where the fatigue crack growth rate is plotted against the SIF values. The used hydrogen pressure was

higher than one chosen for this thesis, but the loading ratios were comparably lower. In this study, the resulting crack growth rates were also notably lower than the values calculated in this thesis. An explanation for this relatively large difference might be the fact that the crack growth rates in the literature are mainly the results of experimental tests, while on the other hand, the equations used to calculate the crack growth rates in this thesis are derived from equations which can be considered to be generalized. In the end, there are a considerable number of factors affecting the crack growth, and it could be that this specific equation is not the most precise for this case study and with different parameters, the results could have been more in line with the literature. All in all, although the crack growth rate calculation results in hydrogen were slightly higher than experimental results found in the literature, the setting was not completely identical, and hydrogen's effect on the crack growth was clearly seen when comparing these results to the crack growth rate in natural gas. It could be stated that the results were more representative of a worst-case scenario.

Another noteworthy area is the FEA results. The software used for the simulation was a student version, which had limitations, especially related to model size, so the meshing could be made denser with a full version of the software. The results should also be verified with some other method if they were to be utilized. On the other hand, since the focus of this thesis was on the crack growth rate plots and the results of FEA were not necessity for forming the plots, since any arbitrary range of values could be used for calculations, it was not necessary.

6 Conclusions

The aim of the Master's thesis was to understand the effect of hydrogen on steel, particularly in a scenario where existing natural gas pipeline is used for transportation of hydrogen. This was done by first getting familiar with the basic theory behind the hydrogen's harmful effects on steel through the literature review. In research part of the work, using a specified example which represented a typical natural gas transmission pipeline with similar dimensions, material, loading properties and other parameters, the aim was to predict the fatigue crack growth rate curves for both natural gas and hydrogenous environments. Hydrogen induced cracking is well known phenomenon and its effect can be clearly seen by comparing the crack growth curves presented in this thesis. Although straight conclusions should not be made, with the example of natural gas pipeline used in the thesis, the difference in crack growth rate is significant with medium changed to hydrogen and should be noted when planning on using existing natural gas pipelines to transport hydrogen. Especially, when considering the inevitable risks of hydrogen leak.

When it comes to further studies, an interesting possibility would be to use FEA software to simulate the crack growth tendencies in hydrogenous environment and see how the results of this thesis compare to the literature-based crack growth results. Life-to-failure analysis with natural gas and hydrogen, both with similar properties, and then comparing the outcomes would also offer a good perspective on hydrogen's effect on steel.

References

Amaro, R., Drexler, E. & Slifka, A. 2013. Fatigue crack growth modeling of pipeline steels in high pressure gaseous hydrogen. In: Kang, G., Sangid, M. & Vormwald, M. International Journal of Fatigue, Vol 62. Amsterdam, Netherlands: Elsevier B.V. 2013. Pp. 249-257.

Ansys, Inc. 2024. Ansys Mechanical (2024 R1) [Computer program]. Ansys, Inc. Available at: https://www.ansys.com/products/structures/ansys-mechanical (Accessed: 25.11.2024).

API Specification 5L. 2018. Line Pipe. 46th edition. Washington, D.C.: Api Publishing Services. 193 p.

Chandra, A., Thodla, R. & Sosa, S. 2023. Fatigue crack growth rate study of new X52 line pipe steel in hydrogen blended methane. Pressure Vessels & Piping Conference: Proceedings of the ASME 2023, Atlanta, Georgia, USA. 16-21.7.2023. Pp. 1-10.

Cheng, Y. F. 2013. Stress Corrosion Cracking of Pipelines. Hoboken, New Jersey: John Wiley & Sons, Inc. 257 p.

Ciaraldi, S. W. 1992. Stress-Corrosion Cracking of Carbon and Low-Alloy Steels (Yield Strengths Less Than 1241 MPa). In: Jones, R. H. Stress-Corrosion Cracking, 4th Edition. Ohio, US: ASM International. 1992. Pp. 41-62.

Darcis, P., Treinen, J. M. & McColskey, J.D. 2009. Fatigue Crack Growth Rates in Pipeline Steels Using Curved M(T) Specimens*. In: Mitchell, M. R. et al. Journal of Testing and Evaluation. Vol 37, No. 6. West Conshohocken, Pennsylvania, US: American Society for Testing and Materials. 2009. Pp. 1-9.

Ferreira, O., Fonseca, A., Adame, C., Bundaleski, N., Robinson, R. & Teodoro, O. 2024. Advancing hydrogen leak detection: Design and calibration of reference leaks. In: Djukic, M. International Journal of Hydrogen Energy, Volume 68. Ofxord, United Kingdom: Elsevier Ltd. 2024. Pp. 1090-1096.

Gavriljuk, V. G., Shyvaniuk, V. M. & Teus, S. M. 2022. Hydrogen in Engineering Metallic Materials: From Atomic-Level Interactions to Mechanical Properties. Cham, Switzerland: Springer Nature Switzerland AG. 290 p.

Goutam, G., Rostron, P., Garg, R. & Panday, A. 2018. Hydrogen induced cracking of pipeline and pressure vessel steels: A review. In: Hutchinson, J. Engineering Fracture Mechanics, Vol. 199. Amsterdam, Netherlands: Elsevier B.V. 2018. Pp. 609-618.

Hayward, E. & Fu, C. 2013. Interplay between hydrogen and vacancies in α-Fe. In: Kamien, R. Physical Review B, Vol. 87. College Park, Maryland: American Physical Society. Pp. 1-14.

Jones, R. H. & Ricker, R. E. 1992. [Chapter 1:] Mechanisms of Stress-Corrosion Cracking. In: Jones, R. H. Stress-Corrosion Cracking, 4th Edition. Ohio, US: ASM International. 1992. Pp. 1-40.

Juan, S., Guo, J., Xing, B., Gao, R. & Hua, Z. 2024. CO2 effect on the fatigue crack growth of X80 pipeline steel in hydrogen-enriched natural gas: Experiment vs DFT. In: Veziroglu, E. International Journal of Hydrogen Energy, Vol. 66. Oxford, United Kingdom: Elsevier Ltd. 2024. Pp. 636-644.

Kot, R. 2001. Hydrogen Attack, Detection, Assessment and Evaluation [web document]. Published 2001 [Referred 26.11.2024]. Available: https://www.ndt.net/article/apcndt01/papers/1154/1154.htm.

Li, X., Ma, X., Zhang, J., Akiyama, E., Wang, Y. & Song, X. 2020. Review of Hydrogen Embrittlement in Metals: Hydrogen Diffusion, Hydrogen Characterization, Hydrogen Embrittlement Mechanism and Prevention. In: Ye, H. Acta Metallurgica Sinica (English Letters), Vol. 33. Beijing, China: The Chinese Society for Metals. 2020. Pp. 759-773.

Mahajan, D., Tan, K., Venkatesh, T., Kileti, P. & Clayton, C. 2022. Hydrogen Blending in Gas Pipeline Networks – A Review. In: Lee, I-H., Tran, D. & Dao, V. Energies, Vol. 15. Basel, Switzerland: MDPI. 2022. Pp. 1-32.

Mohtadi-Bonab, M., Mousavi, H., Pourazizi, R. & Szpunar, J. 2020. Finite element modeling of HIC propagation in pipeline steel with regard to experimental observations. In: Veziroglu, T. International Journal of Hydrogen Energy, Vol. 45, Issue 43. Oxford, United Kingdom: Elsevier Ltd. 2020. Pp. 23122-23133.

Nagumo, M. 2016. Fundamentals of Hydrogen Embrittlement. Singapore, Singapore: Springer Science+Business Media Singapore. 239 p.

Nagumo, M. 2004. Hydrogen related failure of steels – a new aspect. In: Reed, R. Materials Science and Technology, Vol. 20, Issue 8. London, United Kingdom: Maney Publishing. 2004. Pp. 940-950.

Oesterlin, H., Fischer, C. & Michler, T. 2024. Evaluation of Lifetime Predictions for Future Hydrogen Pipelines by Different Fracture Mechanics-Based Design Codes. In: Ravi, S. K. Energy Technology. Weinheim, Germany: Wiley-VCH Verlag GmbH & Co. KGaA. 2024. Pp. 1-13.

Poorhaydari, K. 2021. A Comprehensive Examination of High-Temperatures Hydrogen Attack – A Review of over a Century of Investigations. In: Asthana, R. Journal of Materials Engineering and Performance, Vol. 30, Issue 11. Ohio, US: Springer Science+Business Media. 2021. Pp. 7875-7908.

Polyanskiy, V. A. & Belyaev, A. K. 2021. Advances in Hydrogen Embrittlement Study. Cham, Switzerland: Springer Nature Switzerland AG. 213 p.

Popov, B. N. 2015. Corrosion Engineering: Principles and Solved Problems. Amsterdam, Netherlands: Elsevier B.V. 794 p.

Pugno, N., Ciavarella, M., Cornetti, P. & Carpinteri, A. 2006. A generalized Paris' law for fatigue crack growth. In: Hill, R. Journal of of Mechanics and Physics of Solids, Vol 54. Amsterdam: Netherlands: Elsevier B.V. 2006. Pp. 1333-1349.

Shoji, T. & Raja, V. S. 2011. Stress Corrosion Cracking: Theory and Practice. Cambridge, UK: Woodhead Publishing Limited. 792 p.

Somerday, B.P., Sofronis, P., Nibur, K.A., San Marchi, C. & Kirchheim, R. 2013. Elucidating the variables affecting accelerated fatigue crack growth of steels in hydrogen gas with low oxygen concentrations. In: Rohrer, G. Acta Materialia, Vol 61. Amsterdam, Netherlands: Elsevier B.V. 2013. Pp. 6153-6170.

Télessy, K., Barner, L. & Holz, F. 2024. Repurposing natural gas pipelines for hydrogen: Limits and options from a case study in Germany. In: Veziroglu, E. International Journal of Hydrogen Energy, Vol. 80. United Kingdom: Elsevier Ltd. 2024. Pp. 821-831.

Ugwu, L., Morgan, Y & Ibrahim, H. 2021. Application of density functional theory and machine learning in heterogeneous-based catalytic reactions for hydrogen production. In:

Veziroglu, T. International Journal of Hydrogen Energy, Volume 47, Issue 4. United Kingdom: Elsevier Ltd. 2022. Pp. 2245-2267.